Model Predictive Control for Energy-Efficient HVAC Operation with Humidity and Latent Heat Considerations

Naren Srivaths Raman*, Karthikeya Devaprasad, Bo Chen, Herbert A. Ingley, Prabir Barooah

Department of Mechanical and Aerospace Engineering, University of Florida, Gainesville, FL 32611, USA

Abstract

Even though energy-efficient climate control of commercial buildings using model predictive control (MPC) has been widely investigated, most MPC formulations ignore humidity and latent heat. The inclusion of moisture makes the problem considerably more challenging, primarily since a cooling and dehumidifying coil model which accounts for both sensible and latent heat transfers is needed. In this work, we propose an MPC controller in which humidity and latent heat are incorporated in a principled manner. We construct low order data-driven models of a cooling and dehumidifying coil that can be used in the MPC formulation. The resulting controller's performance is tested in simulation using a plant that differs significantly from the model used by the optimizer. Additionally, the performance of the proposed controller is compared with that of a naive MPC controller which does not explicitly consider humidity, and also to that of a conventional rule-based controller. Simulations show that the proposed MPC controller outperforms the other two in terms of energy use and thermal comfort. It is also observed that the naive MPC formulation which does not consider humidity leads to poor humidity control under certain conditions. Such violations in humidity can adversely affect occupant comfort and health.

Keywords: model predictive control, HVAC systems, humidity, smart buildings, energy efficiency, economic MPC, latent heat.

1. Introduction

The application of Model Predictive Control (MPC) for energy-efficient climate control of buildings has been an active area of research; see the review articles [1, 2] and references therein. In MPC, control commands for a planning horizon are decided at every decision instant by solving an optimization problem, implementing only the first segment of the plan, and then repeating the process ad infinitum. Because of its use of numerical optimization, MPC can handle various constraints that are otherwise challenging to ensure, which has led to the success of MPC in many applications [3].

In case of building climate control, the advantage of MPC over traditional rule-based controllers is that MPC can satisfy conflicting goals such as keeping energy use small while maintaining thermal comfort and indoor air quality. Moreover, most modern day commercial buildings are equipped with powerful controller hardware, communication infrastructure, and sensors needed to implement advanced control algorithms like MPC [1].

Thermal comfort is influenced by several factors such as space temperature, humidity, air speed, clothing, metabolic rate, etc. [4]. Space temperature and humidity are especially important factors in determining comfort and health [5, 6, 7]. Despite the importance of humidity and latent heat in building climate control, it is ignored in most existing MPC formulations.

The principal challenge in including humidity and latent heat is that variables that determine the building's temperature and humidity—humidity and temperature of the conditioned air—are a complex function of control commands, and cannot be independently chosen. The control commands that can be independently chosen are inlet conditions of the cooling coil that cools and dehumidifies the air supplied to the indoor space. Incorporating humidity into MPC requires a model of the cooling and dehumidifying coil that accounts for both *sensible and latent heat transfers*, and predicts how control commands (conditions at the coil inlet) determines the temperature and humidity of the conditioned air. Such models are usually highly complex. Some are partial differential equations (PDEs) with a large number of parameters and several sub-models based on the condition of the cooling coil such as completely dry, completely wet, and partly wet [8]. Some are ordinary differential equations or even static models consisting of a large number of empirical relations that vary depending on coil geometry, configuration, and manufacturer [9, 10]. Such complex models are not suitable for MPC, which involves real-time optimization. In addition, nonlinearities in the humidity dynamics make the

*Corresponding author

Email addresses: narensraman@ufl.edu (Naren Srivaths Raman), kdevaprasad@ufl.edu (Karthikeya Devaprasad), bo.chen@ufl.edu (Bo Chen), hhingley@aol.com (Herbert A. Ingley), pbarooah@ufl.edu (Prabir Barooah)

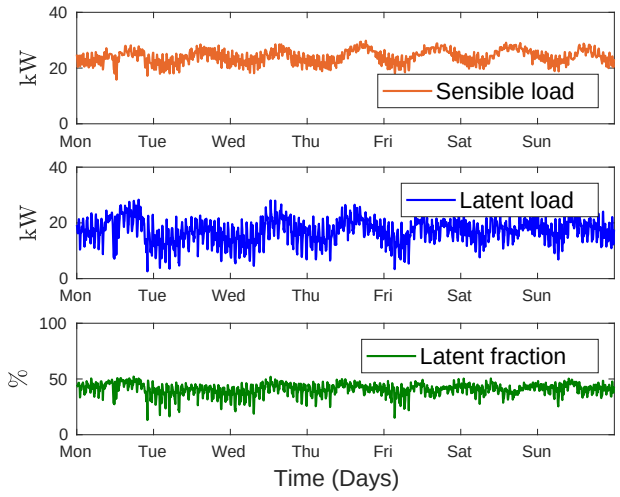

Figure 1: Comparison of sensible load and latent load in a cooling coil for a week. The data was obtained from an air handling unit (AHU-2) serving an auditorium in Pugh Hall at the University of Florida, USA.

underlying optimization problem non-convex [11].

Rule-based controllers that are currently used in practice employ conservatively designed rules that have been arrived at after decades of experience. For instance, a widely used heuristic in hot-humid climates is to keep the conditioned air setpoint at 12.8 °C (55 °F) [12]. This low value ensures the air delivered to the indoor space is dry enough to maintain humidity within allowable limits under worst-case conditions. The downside is that worst-case conditions occur rarely, which leads to high energy use. Not only is the air cooled unnecessarily, but it must then be reheated to prevent the indoor space from becoming too cold. Moreover, rule-based controllers do not take full advantage of the thermal inertia of buildings and thermal comfort range of occupants which could lead to energy savings.

The recent literature on MPC for HVAC (heating, ventilation and air conditioning) system control is focused on energy use minimization while maintaining thermal comfort and indoor air quality [1, 2]. The motivation is the large energy footprint of HVAC systems. An MPC controller which minimizes energy/cost without including humidity and latent heat in its problem formulation could have two potential issues. One, it may lead to poor humidity control. Two, since the latent component of cooling—energy required to dehumidify air—is not accounted for in the objective function, the predicted energy use by the controller may be far from the actual energy use when the controller is used in practice. Figure 1 shows the sensible load, latent load, and the latent fraction (ratio of latent load to the total load) in a cooling coil for a week which was obtained from an air handling unit (AHU-2) serving an auditorium in Pugh Hall at the University of Florida, USA. It can be seen that the latent load is not negligible and constitutes about 41% of the total cooling load.

In this paper, we propose an MPC formulation for energy-efficient climate control of a commercial building in which humidity and latent heat are taken into account in a principled manner. The proposed controller is hereafter referred to as *SL-MPC*, because it accounts for both sensible and latent components of cooling. We specifically focus on a variable-air-volume (VAV) heating, ventilation and air conditioning (HVAC) system that uses chilled water to cool and dehumidify, i.e., condition the air supplied to the building. Figure 2 shows the schematic of a a VAV HVAC system. To avoid clutter, we consider a single zone building, though the proposed method can be extended to multi-zone buildings.

As mentioned earlier, one of the main challenges of including humidity and latent heat is the need for a cooling and dehumidifying coil model that is simple enough to be used in real-time optimization and yet accurate enough to lead to useful results. To address this challenge we develop a data-driven low order model that predicts temperature and humidity of the conditioned air (outputs) as a function of the inputs: the temperature, humidity and flow rate of air incident on the coil, and temperature and flow rate of chilled water entering the coil. This model is used in the optimizer used by the MPC controller. We also develop a slightly more complex, but much higher accuracy, data-driven model that is used to simulate the plant. Both models are identified from data, which can come from experiments or from software such as EnergyPlus [13].

Apart from the proposed MPC controller and the data-driven cooling coil models, a third contribution of the paper is a comparison of the performance of the proposed controller with two other controllers: (i) an MPC controller that does not have humidity constraints and latent heat explicitly accounted for, which is referred to as *S-MPC* since it only accounts for sensible heat, and (ii) a widely used rule-based controller ("single maximum" [14]), which is referred to as *BL* (for *baseline*).

The simulation studies reported here show that the proposed *SL-MPC* controller uses the least amount of energy and meets thermal comfort constraints as well or better, compared to the other two controllers. It is also observed that *S-MPC* makes decisions that lead to poor humidity control under certain conditions. Over long periods of time, this can cause issues such as mold growth, a critical health concern in hot-humid climates [6, 7].

A preliminary version of this work has been reported in [15], wherein we have compared the performance of *SL-MPC* and *BL*. In this paper, we add *S-MPC* to the comparison and quantify their performance in terms of energy consumption and thermal comfort violation. This comparison clarifies the implication of ignoring humidity in the problem formulation: that serious adverse effects can occur. To the best of our knowledge, this paper is the only one that provides a performance comparison of MPC schemes with and without humidity for HVAC systems. Such a comparison is needed to examine the

trade off between the benefit of incorporating humidity into the controller and extra cost of doing so, which comes from the additional sensors and models needed.

The rest of this paper is organized as follows. Section 1.1 reviews the related work on MPC-based building climate control vis-à-vis humidity and latent heat considerations. Section 2 describes a single-zone variable air volume (VAV) HVAC system and the mathematical models we use in simulating the plant (the system to be controlled). Section 3 presents the proposed *SL-MPC* control strategy, and the control-oriented cooling and dehumidifying coil model. It also describes the two other control algorithms used for comparison with the proposed controller. The simulation setup and their results are discussed in Sections 4 and 5 respectively. Concluding remarks are provided in Section 6.

1.1. Review of prior work

There have been several studies in which MPC is used for energy-efficient climate control of buildings—see the review papers [1, 2] and the references therein. However, there are only a few works which have considered humidity explicitly in their MPC problem formulation. We limit ourselves to these references. Based on the objective function to be minimized in the MPC formulation, these works can be classified into two broad categories: (i) economic MPC and (ii) set point tracking MPC. In set point tracking MPC, the objective function is chosen so that minimization of the objective function helps to drive the relevant output(s) to the desired set point. In economic MPC, the objective function is chosen to be a performance measure—usually the economic cost—that may not correspond to a steady state operation as it does in case of set point tracking. See [16, 17] for a through exposition of tracking and economic MPC.

References [18, 19, 20, 21, 22] are examples of setpoint tracking MPC. In [18], an MPC controller is designed to maintain the supply air temperature and humidity at a given set point by varying the mass flow rate of chilled water and inlet water temperature of the heating coil. A two layered control architecture is presented in [19] and [20] for operating direct expansion (DX) cooling systems. The upper layer is an open loop controller while the lower layer is based on MPC. In [21], an aggregated model of the building and HVAC system is obtained with the supply air fan speed and the chilled water valve opening as inputs, and room temperature and relative humidity as outputs. Subsequently, an MPC controller is used to maintain the room temperature and relative humidity at its set point with the above model. Both temperature and humidity are considered in the problem formulation. A control-oriented desiccant wheel model is used in an MPC-based control scheme to regulate humidity in [22].

The MPC controller proposed in this paper, and those in references [23, 24, 25, 26, 27, 28, 29, 30, 31, 32] belong to the category of economic MPC, with total energy use being the objective function to minimize in this work. In [23], it is assumed that the relative humidity of the conditioned air after the cooling coil is always 90%, while [24] assumes both the temperature and the humidity ratio of the conditioned air are constant. These assumptions avoid the need for a cooling coil model though the validity of these assumptions is questionable. Occupancy-based control algorithms are experimentally evaluated in [25]. These algorithms are used to vary the control inputs at the zone-level, while the inputs at the air handling unit are not affected. An economic MPC scheme—for energy use minimization—with humidity and latent heat considerations is presented in [26]. Unlike the chilled water system used in this work, the focus in [26] is on DX cooling systems.

In [27], MPC is used to control a variable refrigerant flow (VRF) based HVAC system. The goal is to minimize economic costs while maintaining the thermal comfort of occupants. Thermal comfort is measured using the predicted mean vote (PMV) index [33, 4]. PMV is dependent on several variables one of which is humidity. Even though humidity is explicitly considered in this work, unlike the chilled water system used in our work, the focus is on a VRF system.

A framework which concurrently optimizes thermal and electric storage in buildings is presented in [32]. The goal of the optimizer is to reduce the operating cost and demand peaks under time-of-use tariffs by varying the temperature setpoints of the zones in a building and battery dispatch. In [28], MPC is used to optimize the performance of a hydronic radiant floor system in an office building. However, the humidity in the building is controlled using a proportional-integral (PI) controller, and is not considered in the MPC formulation.

In [29], MPC is used to control an environmental chamber located at the Pennsylvania State University campus. Humidity is indirectly considered through a data-driven thermal comfort model (dynamic thermal sensation model) developed by the authors. However, latent heat is ignored in the MPC formulation. In [31], a token based scheduling algorithm is used to minimize the energy consumption for a building located at the Nanyang Technological University, Singapore campus. It is based on a distributed control algorithm presented in [34], and is used to vary the supply air flow rate to the zones. Humidity is indirectly maintained through the thermal sensation model used but latent heat is ignored.

Ref. [30] provides a comprehensive MPC framework which uses real-time building energy management system data. An enthalpy control algorithm is used to regulate the amount of outdoor air supplied to a building.

There are also a few papers in which the terms in the objective function consist of both energy use and deviation from set points, so these can be thought of as a hybrid between tracking and economic MPC—[35, 36, 37]. Multiple MPC strategies are

compared for an air handling unit serving a single-zone in [35]. It is assumed that the temperature and humidity ratio after the cooling coil can be chosen independently, thereby not requiring the use of a cooling coil model. This assumption will not hold in physical systems, as the only variables that can be independently chosen are the inlet conditions to the coil. Unlike the cooling-based air dehumidification considered in this work, reference [36] uses a liquid desiccant air conditioning (LDAC) system. The inlet desiccant solution flow rate and temperature are varied to maintain the temperature and humidity ratio of the outlet air.

Ref. [37] is the most relevant to our work; they use a cooling coil model in their optimization in which temperature and humidity of the conditioned air is modeled correctly to be thermodynamically coupled. The supply air flow rate is not a control command, while in our formulation it is. The controller in [37] will be unaware of disturbances in the longer time scales, since a short prediction horizon of 10 minutes is used. In contrast, we use a prediction horizon of 24 hours. Moreover, there are multiple elements included in the objective function: energy use, thermal comfort, indoor air quality, etc., which needs careful tuning of weights. In our formulation, energy use is the objective to be minimized, with thermal comfort and indoor air quality being constraints to be met. Lastly, a nondeterministic optimization algorithm (genetic algorithm) is used to perform the minimization which is challenging to use for real-time control. In contrast, we use a deterministic search method through a nonlinear programming (NLP) solver.

Although the papers on HVAC control that do not consider humidity and latent heat are outside the scope of this review, a subset of those works report experimental evaluations in real buildings. These deserve special attention: if an MPC controller that does not consider humidity and latent heat can still provide good performance in real buildings that are affected by humidity and latent heat, then incorporating these features into the controller—which necessarily increase complexity—is perhaps not necessary. In particular, refs. [38, 39, 40] describe experimental demonstrations that have been carried out with MPC-based controllers on real buildings. The problem formulations in these references do not consider latent heat/room humidity dynamics. It is not clear from the reported assessment if the controllers were able to maintain humidity, since humidity measurements were not reported.

In [38], an MPC based controller was implemented in a Swiss office building. They used thermally activated building systems, an air handling unit, and blinds, for actuation. Majority of the experiments were done when the weather was cold and dry in which humidity and latent cooling loads were unlikely to be of concern. However, one set of experiments was done between May-August when it was hot and humid. Space humidity was not reported in the evaluations. The MPC

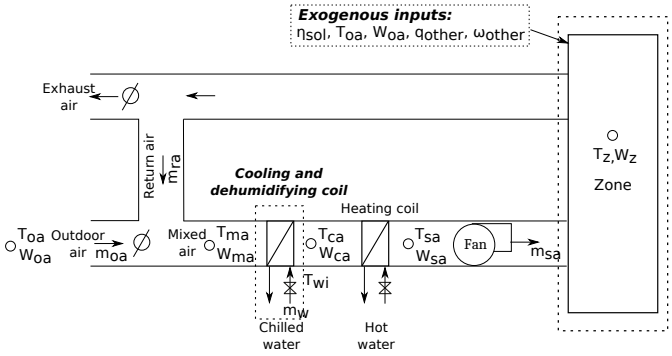

Figure 2: Schematic of a single-zone commercial variable-air-volume HVAC system.

demonstration reported in [39] controlled the heating system of a building in Prague during winter when humidity is not a concern for that climate.

The work [40] describes an MPC-based controller that was implemented in a mid-size ($650m^2$) commercial building in Champaign, Illinois, which is hot and humid during the summer. Two sets of tests were conducted. One was during the transition season in October and the other was during cold season (February). It is not clear from published results whether humidity was maintained within acceptable limits, since only zone temperature and CO_2 levels were reported, not humidity.

In summary, it is not possible to say from the published literature if an MPC controller that does not consider humidity and latent heat is able to provide humidity control. Our results—reported later in the paper—indicate it is unlikely in hot and humid climates, thus motivating a need for an MPC formulation that includes these features.

2. System description and models

Our focus is a single-zone variable-air-volume HVAC system used in commercial buildings. The schematic of a typical configuration used is shown in Figure 2. In such a system, part of the air exhausted from the zone is recirculated and mixed with outdoor air. Then the mixed air is sent through a cooling coil where it is cooled and dehumidified to conditioned air temperature (T_{ca}) and humidity ratio (W_{ca}). This air is then passed through a reheat coil where the air is heated to supply air temperature (T_{sa}) before being supplied to the zone. There is no water vapor phase change across the heating coil, so the humidity ratio of supply air and conditioned air is the same: $W_{sa} = W_{ca}$. The role of the climate control system is to vary the following control commands: (i) supply air flow rate (m_{sa}), (ii) outdoor air ratio (r_{oa}, which is the ratio of outdoor air flow rate to supply air flow rate, $r_{oa} = \frac{m_{oa}}{m_{sa}} = \frac{m_{oa}}{m_{oa}+m_{ra}}$), (iii) conditioned air temperature (T_{ca}), and (iv) supply air temperature (T_{sa}), to maintain thermal comfort and indoor air quality in the zone. So

the control command vector is:

$$u = [m_{sa}, r_{oa}, T_{ca}, T_{sa}]^T \in \Re^4. \quad (1)$$

These four values can be commanded as setpoints to lower level control loops, and thus we treat u as a control command to be decided by the proposed MPC controller. We assume that the controller also has access to the zone dry-bulb temperature and zone humidity measurements in real time; these can be measured using commercially available sensors. The controller will also need prediction of certain exogenous disturbances, which will be described in Section 3.

2.1. Plant model used for simulation assessment

It is convenient to first describe the models that are used to simulate the *plant*, i.e., the system being controlled, since simplified versions of some of the components of the plant are used by the controller to make decisions. In the following subsections we describe these mathematical models. The plant parameters are chosen to mimic a real HVAC system of the type shown in Figure 2, the one that serves a 465 m^2 (5000 sq.ft.) auditorium in Pugh Hall at the University of Florida, USA.

2.1.1. Hygro-thermal dynamics model

We use the following RC (resistor-capacitor) network model for the temperature dynamics of the zone serviced by the HVAC system [41]:

$$C_z \dot{T}_z(t) = \frac{(T_w(t) - T_z(t))}{R_w} + q_{HVAC}(t) + A_e \eta_{sol}(t) + q_{other}(t) \quad (2)$$

$$C_w \dot{T}_w(t) = \frac{(T_{oa}(t) - T_w(t))}{R_z} + \frac{(T_z(t) - T_w(t))}{R_w} \quad (3)$$

where T_z is the zone temperature, T_w is the wall temperature, T_{oa} is the outdoor air temperature, q_{HVAC} is the heat influx due to the HVAC system, η_{sol} is the solar irradiance, q_{other} is the internal heat load due to occupants, lights, equipments, etc., C_z and C_w are the thermal capacitance of the zone and the wall respectively, R_z is the resistance to heat exchange between the outdoors and wall, R_w is the resistance to heat exchange between the wall and indoors and A_e is the effective area of the building. The heat influx due to the HVAC system is a function of the supply air temperature and zone temperature:

$$q_{HVAC}(t) = m_{sa}(t) C_{pa} (T_{sa}(t) - T_z(t)), \quad (4)$$

where m_{sa} is the supply air flow rate and C_{pa} is the specific heat of air at constant pressure.

The dynamics of zone humidity ratio W_z is modeled as:

$$\dot{W}_z(t) = \frac{R_g T_z(t)}{V P^{da}} \left[\omega_{other}(t) + m_{sa}(t) \frac{W_{sa}(t) - W_z(t)}{1 + W_{sa}(t)} \right] \quad (5)$$

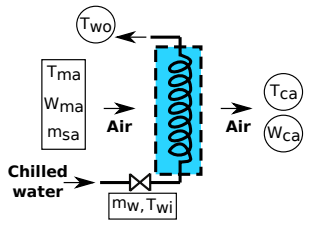

Figure 3: A cooling and dehumidifying coil, and relevant variables (model inputs in rectangles, outputs in circles).

where V is the zone volume, R_g is the specific gas constant of dry air, P^{da} is the partial pressure of dry air, W_{sa} is the supply air humidity ratio, and ω_{other} is the rate of internal water vapor generation due to people and other sources [11].

2.1.2. Cooling and dehumidifying coil model

The inputs for the model are supply air flow rate (m_{sa}), mixed air temperature (T_{ma}), mixed air humidity ratio (W_{ma}), chilled water flow rate (m_w), and inlet water temperature (T_{wi}); see Figure 3. The outputs are conditioned air temperature (T_{ca}) and humidity ratio (W_{ca}).

There is a rich literature on modeling cooling and dehumidifying coils; see [8, 10] and references therein. However, some of these models require coil geometry data which is hard to obtain. Another class of models involve complex partial differential equations [8]. For our purposes a simple static model would suffice as the time constants for a cooling coil are small—about 60 to 120 seconds (see Figures 4 to 7 in [8])—compared to the time constant of zone thermal dynamics, which is in hours [41]. The model used in EnergyPlus (see Section 16.2.1 in [9]) is such a static model. It is still complex and difficult to replicate as it involves many empirical relations. Therefore, we opt for a grey box data-driven model. EnergyPlus is used as a "virtual cooling coil testbed", and data collected from EnergyPlus simulations is used to fit the parameters of the model. The process is explained below.

A single-zone commercial building is simulated in EnergyPlus version 8.9 [13], with a cooling coil pulling in unmixed outdoor air and supplying it to the zone after cooling and dehumidifying it. Using unmixed air ensures that we have full control over the temperature and humidity ratio of air entering the cooling coil, as EnergyPlus allows the use of a custom generated weather file to specify outdoor conditions. The HVAC air loop also contains a variable flow fan motor to control the mass flow rate of air, and the plant loop contains an electric chiller with variable flow pump to control the mass flow rate of water. The inlet and outlet conditions of the cooling coil are measured.

The rates of flow through the pump and fan are varied using Building Controls Virtual Test Bed (BCVTB) [42]. The air flow rate is varied from 0.1705 kg/s (300 ft^3/min) to 4.6 kg/s (8100 ft^3/min) and the water flow rate is varied from 0 kg/s (0

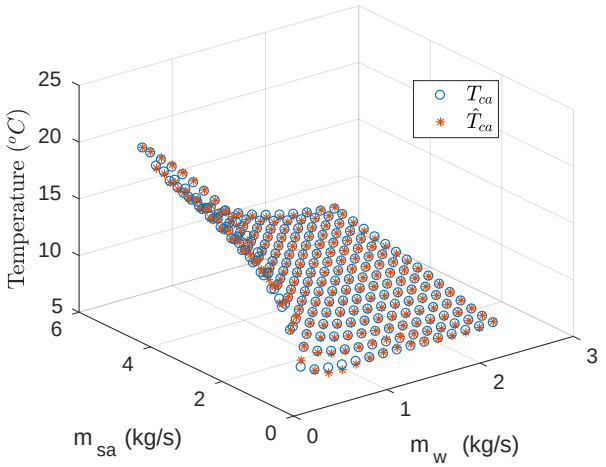

(a) Measured (T_{ca}, output from EnergyPlus simulations) and predicted ($\hat{T}_{ca}$) value of conditioned air temperature for a specific bin, $T_{ma} = 23.9\ ^{\circ}C$ ($75\ ^{\circ}F$) and $RH_{ma} = 50\%$.

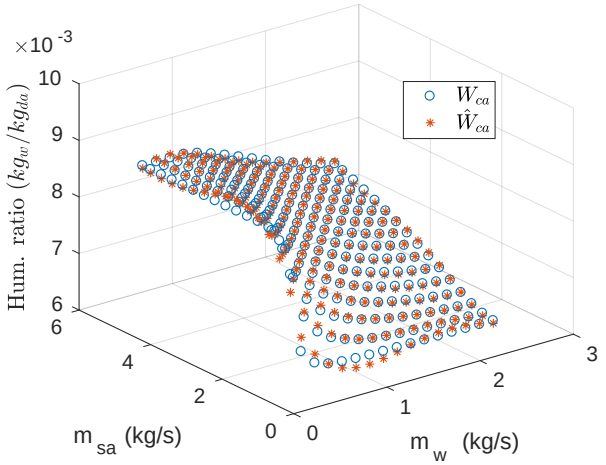

(b) Measured (W_{ca}, output from EnergyPlus simulations) and predicted ($\hat{W}_{ca}$) value of conditioned air humidity ratio for a specfic bin, $T_{ma} = 23.9\ ^{\circ}C$ ($75\ ^{\circ}F$) and $RH_{ma} = 50\%$.

Figure 4: Cooling coil binned model (used in simulating the plant).

$gallons/minute$) to 2.21 kg/s (35 $gallons/minute$). The limits are chosen to mimic the equipment in Pugh Hall. The temperature and humidity ratio of outdoor air are controlled using a custom weather file. Since there are no other components before the coil that interact with outdoor air, we are able to use it to modulate the input conditions to the coil. The temperature is varied from 10 $^{\circ}C$ (50 $^{\circ}F$) to 43.3 $^{\circ}C$ (110 $^{\circ}F$) with steps of 0.56 $^{\circ}C$ (1 $^{\circ}F$). The relative humidity is varied from 10 % to 100 % with steps of 5 %. The model is calibrated using 296,704 data points generated by varying inputs. A separate data set is generated for model validation.

We observe from our initial attempts that for a *fixed* mixed air temperature and relative humidity, the outputs T_{ca} and W_{ca} can be predicted quite well by modeling them as polynomial functions of the mass flow rates of chilled water and supply air. Figure 4 shows an example, using a 5^{th} degree polynomial. However, a single polynomial leads to large errors when used at different mixed air temperatures and relative humidities. We therefore bin the inputs according to T_{ma} and RH_{ma} into 1159 bins, and use a 5^{th} degree polynomial model for each bin. The resulting model is called a "binned model". The root mean square error for the validation data is less than 0.28 $^{\circ}C$ (0.5 $^{\circ}F$, 1%) for T_{ca} and $0.3 \times 10^{-4}\ kg_w/kg_{da}$ (1%) for W_{ca}.

2.1.3. Power consumption models

We assume that the power consumed by components such as dampers is negligible; the only power consuming components are the air supply fan, the reheat coil, and the cooling coil. The fan power is usually modeled as a quadratic function of the supply air flow rate [43]:

$$P_{fan} = \alpha_f m_{sa}(t)^2. \tag{6}$$

The power consumed by the cooling and dehumidifying coil is modeled as being proportional to the heat it extracts from the mixed air stream as follows:

$$P_{cc}(t) = \frac{m_{sa}(t)\left[h_{ma}(t) - h_{ca}(t)\right]}{\eta_{cc} COP_c}, \tag{7}$$

where $h_{ma}(t)$ and $h_{ca}(t)$ are the specific enthalpies of the mixed and supply air respectively, η_{cc} is the cooling coil efficiency, and COP_c is the chiller coefficient of performance. Since a part of the return air is mixed with the outside air, the specific enthalpy of the mixed air is:

$$h_{ma}(t) = r_{oa}(t) h_{oa}(t) + (1 - r_{oa}(t)) h_z(t), \tag{8}$$

where $h_{oa}(t)$ and $h_z(t)$ are the specific enthalpies of the outdoor and zone air respectively, and $r_{oa}(t)$ is the outside air ratio: $r_{oa}(t) := \frac{m_{oa}(t)}{m_{sa}(t)}$. The specific enthalpy of moist air with temperature T and humidity ratio W is given by [44]: $h(T,W) = C_{pa}T + W(g_{H_2 0} + C_{pw}T)$, where $g_{H_2 0}$ is the heat of evaporation of water at 0 $^{\circ}C$, and C_{pa}, C_{pw} are specific heat of air and water at constant pressure.

The power consumed by the reheat coil is modeled as being proportional to the heat added to the conditioned air stream by the coil. Since the humidity ratio does not change across the reheat coil ($W_{sa} = W_{ca}$), the power consumption has the form

$$P_{reheat}(t) = \frac{m_{sa}(t) C_{pa}\left[T_{sa}(t) - T_{ca}(t)\right]}{\eta_{reheat} COP_h}, \tag{9}$$

where η_{reheat} is the reheat coil efficiency, and COP_h is the boiler coefficient of performance.

3. Control algorithms

3.1. Proposed controller: SL-MPC

Figure 5 shows the control architecture for the proposed *SL-MPC* controller. Control decisions are computed in discrete time indices $k = 0, 1, \ldots$, with Δt being the sampling interval.

The control inputs for N time steps are obtained by solving a constrained optimization problem of minimizing the energy consumption subject to thermal comfort, indoor air quality, and actuator constraints. Then the control inputs obtained for the first time step are applied to the plant. The optimization problem is solved again for the next N time steps with the initial state of the model obtained from plant measurements. This process is repeated at the next time instant. To describe the optimization problem, first we define the state vector $x(k)$ and the vector of control commands and internal variables $v(k)$ as:

$$x(k) := [T_z(k), W_z(k)]^T \in \Re^2,$$
$$v(k) := [u(k)^T, m_w(k), W_{ca}(k)]^T \in \Re^6,$$

where $u(k)$ is the control command vector defined in (1). The exogenous input vector is:

$$w(k) := [\eta_{sol}(k), T_{oa}(k), W_{oa}(k), q_{other}(k), \omega_{other}(k)]^T \in \Re^5. \tag{10}$$

At time index j, the decision variables in the optimization problem underlying the proposed MPC controller are denoted by X and V, where $X = [x^T(j+1), x^T(j+2), \ldots, x^T(j+N)]^T$ and $V = [v^T(j), v^T(j+1), \ldots, v^T(j+N-1)]^T$. The predictions of the exogenous inputs $W = [w^T(j), w^T(j+1), \ldots, w^T(j+N-1)]^T$ are assumed known at time index j. In simulations reported later, we use $\Delta t = 5$ minutes and prediction/planning horizon of $N = 288$ (corresponding to 24 hours).

The optimization problem at time index j is:

$$\min_{V,X} \sum_{k=j}^{j+N-1} \Big[P_{fan}(k) + P_{cc}(k) + P_{reheat}(k) \Big] \Delta t, \tag{11}$$

where P_{fan}, P_{cc} and P_{reheat} are given by (6), (7) and (9) respectively, and is subject to the following constraints:

$$T_z(k+1) = T_z(k) + \frac{\Delta t}{C} \Bigg[\frac{(T_{oa}(k) - T_z(k))}{R} + q_{HVAC}(k) + A_e \eta_{sol}(k) + q_{other}(k) \Bigg], \tag{12a}$$

$$W_z(k+1) = W_z(k) + \frac{\Delta t R_g T_z(k)}{V P^{da}} \Bigg[\omega_{other}(k) + m_{sa}(k) \frac{W_{sa}(k) - W_z(k)}{1 + W_{sa}(k)} \Bigg], \tag{12b}$$

$$T_{ca}(k) = f_{co}\big(T_{ma}(k), W_{ma}(k), m_{sa}(k), m_w(k)\big), \tag{12c}$$
$$W_{ca}(k) = g_{co}\big(T_{ma}(k), W_{ma}(k), m_{sa}(k), m_w(k)\big), \tag{12d}$$
$$T_z^{low}(k) \le T_z(k) \le T_z^{high}(k), \tag{12e}$$
$$W_z^{low}(k) \le W_z(k) \le W_z^{high}(k), \tag{12f}$$
$$m_{sa}(k+1) \le min\big(m_{sa}(k) + m_{sa}^{rate}\Delta t, m_{sa}^{high}\big), \tag{12g}$$
$$m_{sa}(k+1) \ge max\big(m_{sa}(k) - m_{sa}^{rate}\Delta t, m_{sa}^{low}\big), \tag{12h}$$
$$r_{oa}(k+1) \le min\big(r_{oa}(k) + r_{oa}^{rate}\Delta t, r_{oa}^{high}\big), \tag{12i}$$
$$r_{oa}(k+1) \ge max\big(r_{oa}(k) - r_{oa}^{rate}\Delta t, r_{oa}^{low}\big), \tag{12j}$$
$$T_{ca}(k+1) \le min\big(T_{ca}(k) + T_{ca}^{rate}\Delta t, T_{ma}(k+1)\big), \tag{12k}$$
$$T_{ca}(k+1) \ge max\big(T_{ca}(k) - T_{ca}^{rate}\Delta t, T_{ca}^{low}\big), \tag{12l}$$
$$T_{sa}(k+1) \le min\big(T_{sa}(k) + T_{sa}^{rate}\Delta t, T_{sa}^{high}\big), \tag{12m}$$
$$T_{sa}(k+1) \ge max\big(T_{sa}(k) - T_{sa}^{rate}\Delta t, T_{ca}(k+1)\big), \tag{12n}$$
$$W_{ca}(k) \le W_{ma}(k), \tag{12o}$$

where constraints (12a)-(12d) and (12o) are for $k = j, \ldots, j+N-1$, constraints (12e) and (12f) are for $k = j+1, \ldots, j+N$, and constraints (12g)-(12n) are for $k = j, \ldots, j+N-2$.

The constraint (12a) is due to the thermal dynamics of the zone, which is a discretized form of a first-order RC network model where R is the resistance to heat exchange between outdoors and indoors, and C is the thermal capacitance of the zone. Note that this is a simpler model of building hygro-thermal dynamics than that used in the plant simulation. The constraint (12b) is due to the zone humidity dynamics which is a discretized form of (5) presented in Section 2.1.1.

Constraints (12c) and (12d) are for the cooling and dehumidifying coil model which is presented in the next subsection (Section 3.1.1).

Constraints (12e) and (12f) are thermal comfort constraints: they specify the range in which the zone temperature and humidity ratio can vary without compromising occupants' comfort. The upper and lower limits for these vary based on the scheduled hours of occupancy. Usually the limits during unoccupied mode (unocc) are relaxed when compared to the occupied mode (occ), i.e. $[T_z^{low,occ}, T_z^{high,occ}] \subseteq [T_z^{low,unocc}, T_z^{high,unocc}]$, $[W_z^{low,occ}, W_z^{high,occ}] \subseteq [W_z^{low,unocc}, W_z^{high,unocc}]$, as shown in Figure 7.

Constraints (12g) and (12h) are to take into account the capabilities of the fan. The minimum allowed value for the supply air flow rate is computed based on the ventilation requirements specified in ASHRAE 62.1 [45] as well as to maintain positive building pressurization. ASHRAE 62.1 demands ventilation based on two factors: number of people and floor area. Positive pressurization is required as dehumidification results in a drop in indoor vapor pressure. This negative pressure gradient may cause the infiltration of moisture from outside, especially if the building envelope is not airtight [44]. The minimum allowed supply air flow rate is:

$$m_{sa}^{low} = max\ \big((m_{oa}^p n_p + m_{oa}^A A)/r_{oa},\ m_{oa}^{bp}/r_{oa} \big), \tag{13}$$

where m_{oa}^p is the outdoor air rate required per person, n_p is the number of people, m_{oa}^A is the outdoor air required per zone area, A is the zone area, m_{oa}^{bp} is the outdoor air rate required to maintain positive building pressurization, and r_{oa} is the outdoor air ratio.

Constraints (12i)-(12n) are to take into account the capabilities of the damper actuators, cooling and reheat coils. In constraints (12k) and (12o) the inequalities $T_{ca}(k+1) \le T_{ma}(k+1)$ and $W_{ca}(k) \le W_{ma}(k)$ ensure that the cooling coil can only cool

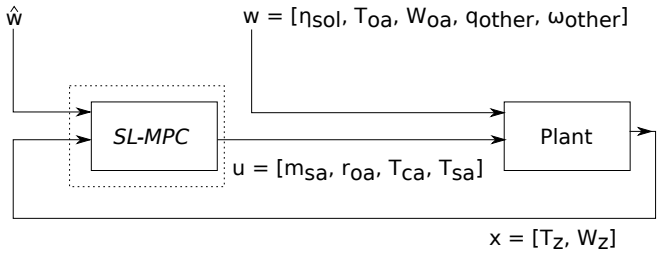

Figure 5: Proposed *SL-MPC*, control architecture.

and dehumidify the mixed air stream; it cannot add heat or moisture. Similarly, in constraint (12n) the inequality $T_{sa}(k+1) \geq T_{ca}(k+1)$ ensures that the reheat coil can only add heat; it cannot cool.

3.1.1. Cooling and dehumidifying coil model used in SL-MPC

Even though the binned model of cooling and dehumidifying coil presented in Section 2.1.2 is quite accurate, it cannot be used in the optimizer as doing so makes the optimization a mixed integer nonlinear programming (MINLP) problem which is quite challenging to solve. Therefore, we develop a control-oriented cooling and dehumidifying coil model which makes the optimization problem a nonlinear program (NLP). It is a static model with the outputs being a polynomial function of the inputs. Note that when the chilled water flow rate is zero, no cooling or dehumidifying of the air can occur so that the conditioned air temperature and humidity ratio must be equal to the mixed air temperature and humidity ratio: $T_{ca} = T_{ma}$ and $W_{ca} = W_{ma}$, when $m_w = 0$. To make the model have this behavior, the following functional form is chosen:

$$T_{ca} = T_{ma} + m_w\, f(T_{ma}, W_{ma}, m_{sa}, m_w) \tag{14}$$

$$W_{ca} = W_{ma} + m_w\, g(T_{ma}, W_{ma}, m_{sa}, m_w) \tag{15}$$

For the functions f and g, we use a quadratic form as higher degree polynomials did not show substantial gain in accuracy. The final form of the model is:

$$\begin{aligned} T_{ca} &= f_{co}(T_{ma}, W_{ma}, m_{sa}, m_w) \\ &= T_{ma} + m_w\big[\alpha_1 T_{ma} + \alpha_2 W_{ma} + \alpha_3 m_{sa} + \alpha_4 m_w + \alpha_5 + \\ &\quad \alpha_6 T_{ma}^2 + \alpha_7 W_{ma}^2 + \alpha_8 m_{sa}^2 + \alpha_9 m_w^2 + \\ &\quad \alpha_{10} T_{ma} W_{ma} + \alpha_{11} W_{ma} m_{sa} + \alpha_{12} m_{sa} m_w + \alpha_{13} m_w T_{ma} + \\ &\quad \alpha_{14} T_{ma} m_{sa} + \alpha_{15} W_{ma} m_w\big] \end{aligned} \tag{16}$$

$$\begin{aligned} W_{ca} &= g_{co}(T_{ma}, W_{ma}, m_{sa}, m_w) \\ &= W_{ma} + m_w\big[\beta_1 T_{ma} + \beta_2 W_{ma} + \beta_3 m_{sa} + \beta_4 m_w + \beta_5 + \\ &\quad \beta_6 T_{ma}^2 + \beta_7 W_{ma}^2 + \beta_8 m_{sa}^2 + \beta_9 m_w^2 + \\ &\quad \beta_{10} T_{ma} W_{ma} + \beta_{11} W_{ma} m_{sa} + \beta_{12} m_{sa} m_w + \beta_{13} m_w T_{ma} + \\ &\quad \beta_{14} T_{ma} m_{sa} + \beta_{15} W_{ma} m_w\big], \end{aligned} \tag{17}$$

where the α_i's and β_j's are the model parameters to be determined. For the numerical results shown next, data obtained from EnergyPlus simulations—as explained in Section 2.1.2—are used to fit these parameters. In practice, measurements can be used to fit them. For the validation data set, the maximum prediction errors observed are 1.61 $^\circ C$ (3 $^\circ F$) and 1.1×10^{-3} kg_w/kg_{da} for T_{ca} and W_{ca}, respectively. This is twice the maximum error observed when using the binned cooling and dehumidifying coil model presented in Section 2.1.2.

3.2. Model predictive control incorporating only sensible heat (S-MPC)

This controller is similar to the one described in Section 3.1, with the main difference being that the moisture and latent heat of the air are not considered. The optimization problem formulation is similar to the one presented in [46].

For this controller, the vectors $x(k)$ and $v(k)$ are defined as follows: $x(k) := T_z(k) \in \Re^1$ and $v(k) := u(k) \in \Re^4$, where $u(k)$ is the control command vector defined in (1). The optimization problem at time index j is:

$$\min_{V,X} \sum_{k=j}^{j+N-1} \Big[P_{fan}(k) + P_{cc}(k) + P_{reheat}(k)\Big]\Delta t, \tag{18}$$

subject to the constraints: (12a),(12e), (12g)-(12n), where P_{fan} and P_{reheat} are given by (6) and (9), and

$$P_{cc}(t) = \frac{m_{sa}(t) C_{pa}\big[T_{ma}(t) - T_{ca}(t)\big]}{\eta_{cc} COP_c}, \tag{19}$$

where $T_{ma}(t)$ and $T_{ca}(t)$ are the dry bulb temperatures of the mixed and conditioned air. The exogenous disturbance needed to compute the constraints in the optimizer are:

$$w(k) := [\eta_{sol}(k), T_{oa}(k), W_{oa}(k), q_{other}(k)]^T \in \Re^4. \tag{20}$$

Notice the difference with *SL-MPC*: since this controller does not consider humidity and latent heat, the constraints placed on the humidity ratio at various locations in the air loop as well as the zone—(12b), (12f), and (12o)—are no longer used. The constraints placed on the system due to the cooling and dehumidifying coil model—(12c) and (12d)—are also not present. *The cooling power term in the objective function is based only on the sensible heat; latent heat is ignored.*

3.3. Baseline control (BL)

The baseline controller—against which the performance of the proposed *SL-MPC*, and *S-MPC* is compared—is chosen to be the single maximum controller that is widely used in practice [14]. In single maximum control, whose schematic representation is shown in Figure 6, the HVAC system operates in three modes based on the zone temperature: cooling, heating, and deadband. When the zone temperature is above the cooling set point for more than 5 minutes the system is in cooling mode and the supply air flow rate (m_{sa}) is varied between the

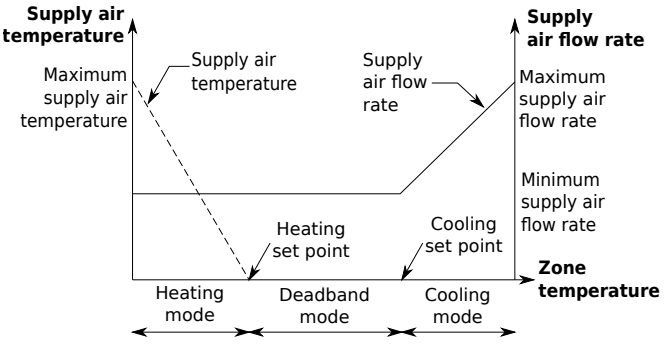

Figure 6: Schematic of Single Maximum control algorithm.

minimum and maximum allowed values to maintain the zone temperature. Similarly, when the zone temperature is below the heating set point for more than 5 minutes the supply air temperature (T_{sa}) is varied to maintain the zone temperature. In this mode the supply air flow rate is kept at the minimum allowed value. Finally when the temperature is between the cooling and heating set points the system is in deadband mode with the supply air flow rate kept at the minimum and the supply air temperature is equal to the conditioned air temperature (T_{sa}=T_{ca}). The minimum allowed value for the supply air flow rate should satisfy the following conditions: one, the ventilation requirements specified by ASHRAE 62.1 [45] and positive building pressurization, as described in Section 3.1. Two, it should be high enough to meet the design heating load at a supply air temperature that is low enough to prevent stratification (e.g., 30 $^{\circ}C$). The outdoor air ratio and the conditioned air temperature are kept constant at all times.

3.4. Information requirement for implementation

All three controllers studied make decisions for the same four control commands in the vector u; see (1). The proposed SL-MPC controller needs real-time measurements of zone temperature and humidity, while the S-MPC and BL controllers need real-time measurements of zone temperature alone. BL controller does not need any predictions, while both the MPC controllers need prediction of the exogenous disturbances, w, over the prediction horizon. Most of these predictions are directly available from weather forecasts. The exceptions are internal heat gains (needed by both MPC schemes), and internal moisture generation (needed by SL-MPC alone). Predictions for these signals can be obtained from occupancy schedules, or from time-series models fitted to estimated heat gains and moisture generation rates that are estimated from temperature and humidity measurements by using methods such as those in [41].

The BL controller does not need any models while both the MPC controllers do. These models are learned off-line. Both the MPC controllers need models of the thermal dynamics of the zone; its parameters can be identified off-line by one of several existing methods. The parameters used in this paper are fitted to Pugh Hall data by using the method in [41]. The SL-MPC requires a humidity dynamic model of the zone and a cooling coil model while the S-MPC does not. The humidity dynamic model used in this paper is a physics-based model; volume of the zone is the only parameter and was obtained from the mechanical drawings for the Pugh Hall building. The cooling coil model parameters can be fitted by a regression technique, to data collected from an actual HVAC system or a high fidelity simulation. The parameters used in this paper are fitted using least squares to data collected from an EnergyPlus model of an AHU. The EnergyPlus model was created using manufacturer provided data about the Pugh Hall equipment; see Section 2.1.2.

4. Simulation setup

The plant is simulated in SIMULINK. The optimization problem is solved using CasADi [47] and IPOPT [48], a nonlinear programming (NLP) solver, on a Desktop Linux computer with 16GB RAM and a 3.60 GHz $\times$ 8 CPU. On an average it takes 2 seconds for *SL-MPC* and 0.6 seconds for *S-MPC* to solve their respective optimization problems. The higher computation time for *SL-MPC* is attributed to the larger number of decision variables. Both the NLPs are non-convex, and the NLP solver indicates that it is able to find a local minimum successfully 100% of the time. In cases where they may not be feasible, the controllers are programmed to use the control command computed at the previous time step.

Three types of outdoor weather conditions are tested: hot-humid (Aug/06/2016), mild (Mar/25/2016), and cold (Dec/20/-2016), all for Gainesville, FL, USA. The weather data is obtained from Weather Underground [49] and National Solar Radiation Database [50]. The simulations are run for 24 hours starting at 8:00 AM.

4.1. Plant parameters and thermal comfort envelope

The plant parameters are chosen based on a large classroom/auditorium ($\sim 6\ m$ high, floor area of $\sim 465\ m^2$) in Pugh Hall located at the University of Florida campus. The RC network parameters are chosen to be $R_z = 0.6 \times 10^{-3}\ ^{\circ}C/W$, $R_w = 0.55 \times 10^{-3}\ ^{\circ}C/W$, $C_z = 3.132 \times 10^7\ J/^{\circ}C$, $C_w = 7.092 \times 10^7\ J/^{\circ}C$, and $A_e = 8.12\ m^2$ from [41], which were obtained by fitting the model to measured data from the building. Volume of the zone (V) is 2831.7 m^3 and was obtained from mechanical drawings for the building. The scheduled occupancy is between 8:00 AM to 5:00 PM during which the following constraints are used: $T_z^{low,occ} = 21.1\ ^{\circ}C\ (70\ ^{\circ}F)$, $T_z^{high,occ} = 23.3\ ^{\circ}C\ (74^{\circ}F)$, $W_z^{low,occ} = 0.0046\ kg_w/kg_{da}$, and $W_z^{high,occ} = 0.0104\ kg_w/kg_{da}$. The unoccupied hours are between 5:00 PM to 8:00 AM during which the constraints are: $T_z^{low,unocc} = 18.9\ ^{\circ}C\ (66\ ^{\circ}F)$, $T_z^{high,unocc} = 25.6\ ^{\circ}C\ (78\ ^{\circ}F)$, $W_z^{low,unocc} = 0.0046\ kg_w/kg_{da}$, and $W_z^{high,unocc} = 0.0104\ kg_w/kg_{da}$. The chosen thermal comfort envelope is shown in Figure 7.

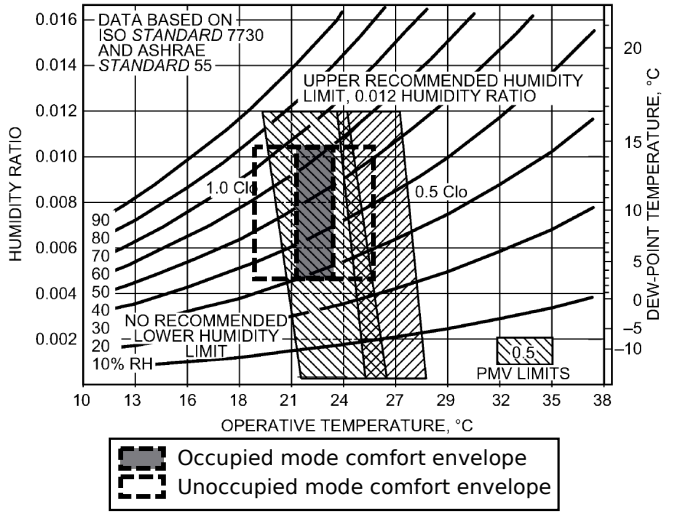

Figure 7: Thermal comfort envelope from [44] shown as the hatched areas. Comfort envelope chosen in this paper shown as the shaded area during scheduled hours of occupancy and the unshaded area enclosed by dashed line during unoccupied hours.

The values for $m_{oa}^{p} = 0.0043\ kg/s/person\ (7.5\ cfm/person)$ and $m_{oa}^{A} = 3.67 \times 10^{-4}\ kg/s/m^2\ (0.06\ cfm/ft^2)$ are chosen based on ASHRAE 62.1 [45] for a lecture classroom. For positive pressurization, $m_{oa}^{bp} = 0.1894\ kg/s$ is chosen so that there are 0.2 air changes per hour. q_{other} and ω_{other} are computed based on the number of people in the zone, assuming that each person produces 100 W of heat and $1.39 \times 10^{-5}\ kg/s$ (50 g/hr) of water vapor [44], with n_p being 175, which is the design occupancy for the building. For q_{other}, an additional heat load of 6000 W is considered based on lighting/equipment power density of 12.92 W/m^2 (1.2 W/ft^2).

4.2. Controller parameters

The controller parameters for *SL-MPC* and *S-MPC* are listed in Table 1. For the 1R-1C model used in the *SL-MPC* and *S-MPC*, we use $R = 1.15 \times 10^{-3}\ ^\circ C/W$ and $C = 6.0167 \times 10^7\ J/^\circ C$. These values are obtained by creating a 1R-1C model equivalent to the 2R-2C model (2), and equating the DC gains and rise times for the transfer functions, with T_{oa} and the heat gains as inputs and the zone temperature as output. As mentioned earlier, $\Delta t = 5$ minutes and $N = 288$ (corresponding to prediction/planning horizon of 24 hours). The number of decision variables for *SL-MPC* is 2304 ($= 288 \times 8$) and *S-MPC* is 1440 ($= 288 \times 5$).

For the baseline controller, outdoor air ratio is kept at 30% and conditioned air temperature is kept at 12.8 $^\circ C$ (55 $^\circ F$).

4.3. Performance metrics

To evaluate the various controllers in this study, we look at the energy consumed by each of them as well as the violations caused with respect to thermal comfort limits specified in Section 4.1.

Table 1: Parameters used in the MPC controllers.

Parameter	Notation	Value	Unit
Maximum allowed supply air flow rate	m_{sa}^{high}	4.6	kg/s
Minimum allowed outdoor air ratio	r_{oa}^{low}	0	%
Maximum allowed outdoor air ratio	r_{oa}^{high}	100	%
Minimum allowed conditioned air temperature	T_{ca}^{low}	12.8	$^\circ C$
Maximum allowed supply air temperature	T_{sa}^{high}	30	$^\circ C$
Maximum allowed rate of change of supply air flow rate	m_{sa}^{rate}	0.37	$kg/s/min$
Maximum allowed rate of change of outdoor air ratio	r_{oa}^{rate}	6	$\%/min$
Maximum allowed rate of change of conditioned air temperature	T_{ca}^{rate}	0.56	$^\circ C/min$
Maximum allowed rate of change of supply air temperature	T_{sa}^{rate}	0.56	$^\circ C/min$
Sampling interval	Δt	5	min

The total energy consumed by the controllers for 24 hours is computed as follows:

$$E_{total} = \int_{24hrs} P_{fan}(t) + P_{cc}(t) + P_{reheat}(t)\, dt, \tag{21}$$

where P_{fan}, P_{cc}, and P_{reheat} are computed using (6), (7), and (9) respectively.

We define the daily temperature violation as:

$$V_T = \int_{24hrs} \Delta T_z(t) dt, \tag{22}$$

where the term $\Delta T_z(t)$ is defined as [24]:

$$\Delta T_z(t) = \begin{cases} T_z(t) - T_z^{high}, & \text{if } T_z(t) > T_z^{high} \\ T_z^{low} - T_z(t), & \text{if } T_z(t) < T_z^{low} \\ 0, & \text{otherwise.} \end{cases} \tag{23}$$

The unit of V_T is $^\circ C$-hours. Similarly, we define the daily humidity violation as:

$$V_W = \int_{24hrs} \Delta W_z(t) dt, \tag{24}$$

where the term $\Delta W_z(t)$ is defined as [24]:

$$\Delta W_z(t) = \begin{cases} W_z(t) - W_z^{high}, & \text{if } W_z(t) > W_z^{high} \\ W_z^{low} - W_z(t), & \text{if } W_z(t) < W_z^{low} \\ 0, & \text{otherwise.} \end{cases} \tag{25}$$

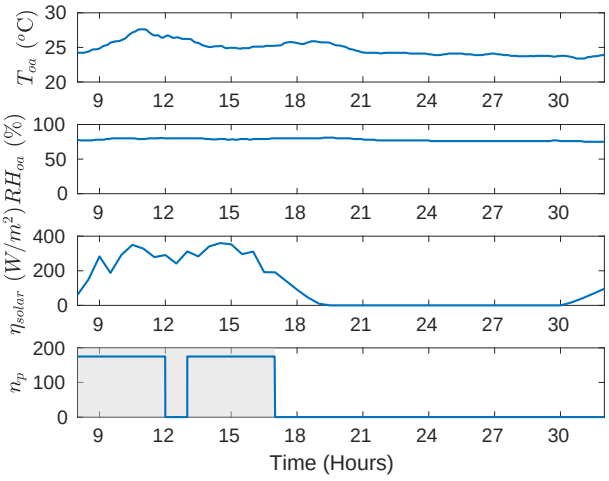

(a) Outdoor weather data and occupancy profile used in simulations (outdoor air temperature, outdoor air relative humidity, solar irradiance, and number of people).

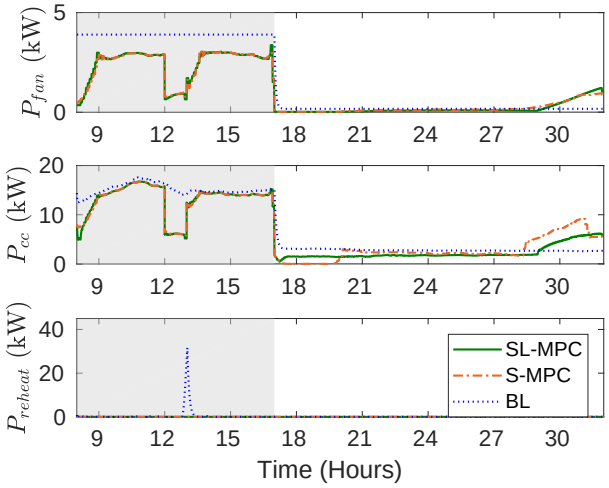

(b) Comparing the power consumptions (fan, cooling, and reheat power).

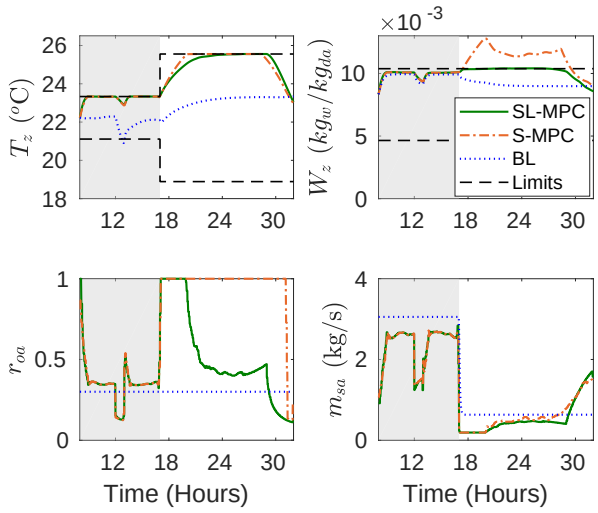

(c) Zone and air loop conditions with the black dashed lines showing the upper and lower comfort limits (zone air temperature, zone air humidity ratio, outdoor air ratio, and supply air flow rate).

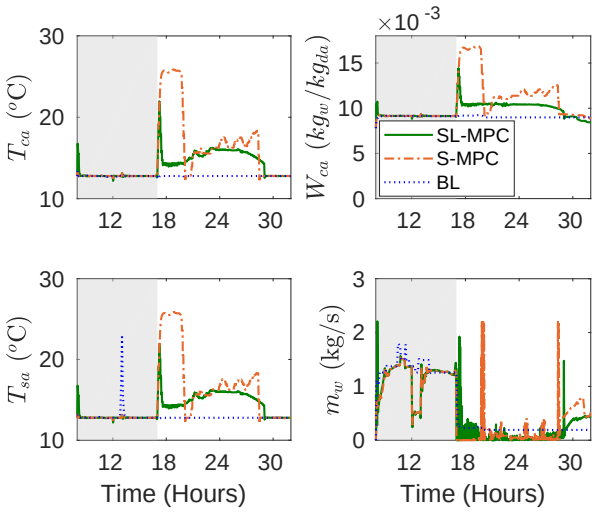

(d) HVAC system conditions (conditioned air temperature, conditioned air humidity ratio, supply air temperature, and chilled water flow rate).

Figure 8: Comparison of the three controllers for a hot-humid day (August/06/2016, Gainesville, Florida, USA). The scheduled hours of occupancy are shown as the gray shaded area.

The unit of V_W is kg_w/kg_{da}-hours.

The larger V_T and V_W are, greater the adverse impact on occupants' comfort and health.

5. Results and discussions

5.1. Results for the different outdoor weather conditions

5.1.1. Hot-humid day

Figure 8 shows the simulation results for a hot-humid day. It is found that *SL-MPC* consumes the least amount of energy when compared to *S-MPC* and *BL*, as presented in Figure 10. There are large violations in humidity limits by *S-MPC*, specifically during the unoccupied hours, as shown in Figures 10 and 8(c).

All three controllers are able to maintain thermal comfort limits during scheduled hours of occupancy almost all the time; see 08:00-17:00 hours in Figure 8(c). The *BL* ensures that dry air is supplied to the zone and hence the humidity limit is not violated since it keeps the conditioned air temperature at a constant value of 12.8 $°C$ (55$°F$). In the case of *S-MPC*, the optimal control decisions made by it are observed to be similar to those made by *SL-MPC*. This can be attributed to the high internal heat load and hot outdoor air temperature. Specifically, *S-MPC* decides to keep the conditioned air temperature low enough (at 12.8 $°C$) to meet the heat load which has the unintended, but

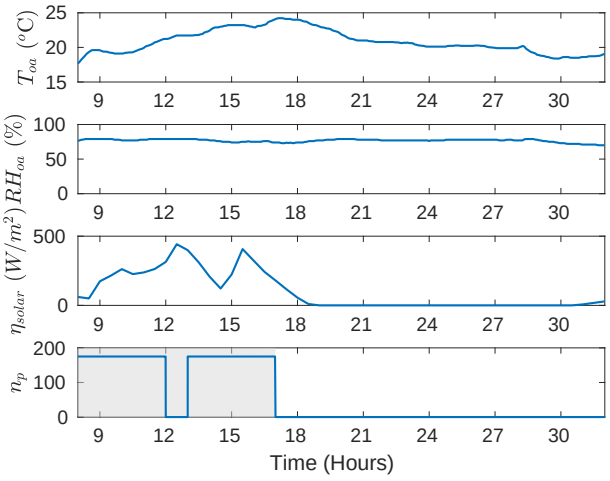

(a) Outdoor weather data and occupancy profile used in simulations (outdoor air temperature, outdoor air relative humidity, solar irradiance, and number of people).

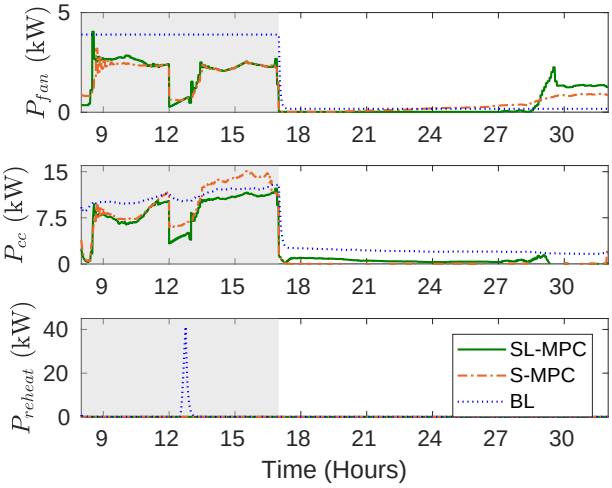

(b) Comparing the power consumptions (fan, cooling, and reheat power).

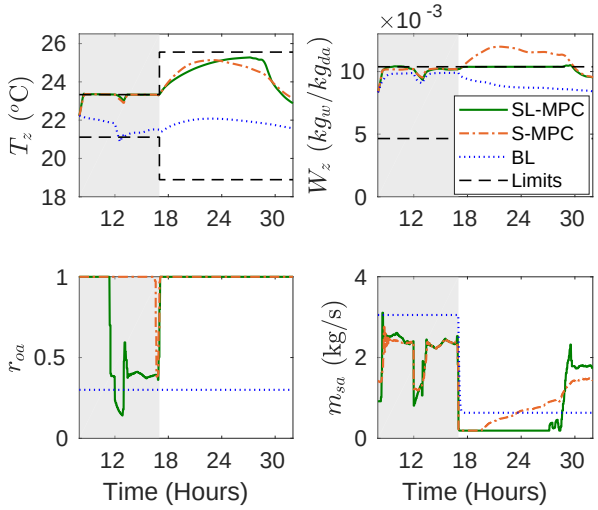

(c) Zone and air loop conditions with the black dashed lines showing the upper and lower comfort limits (zone air temperature, zone air humidity ratio, outdoor air ratio, and supply air flow rate).

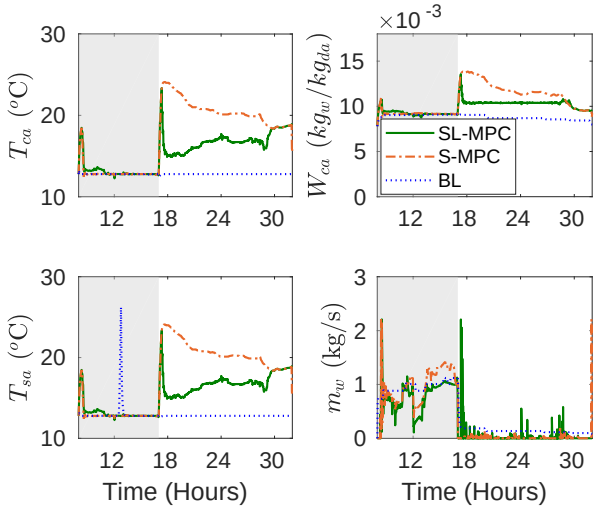

(d) HVAC system conditions (conditioned air temperature, conditioned air humidity ratio, supply air temperature, and chilled water flow rate).

Figure 9: Comparison of the three controllers for a mild day (March/25/2016, Gainesville, Florida, USA). The scheduled hours of occupancy are shown as the gray shaded area.

good, side effect of maintaining zone humidity within the comfort limits.

Both the MPC controllers consume lesser energy when compared to *BL* during occupied hours; see 08:00-17:00 hours in Figure 8(b). The reason for this is that the outdoor air ratio is kept constant for *BL* and it also assumes full occupancy from 08:00 to 17:00 hours. Therefore, the air flow rate has to be kept high enough so that the ventilation requirements specified in ASHRAE 62.1 [45] are met. This high air flow rate, combined with the low conditioned air temperature, is highly suboptimal, especially when there is a reduction in occupancy: not only is the air cooled unnecessarily, but reheating must also be performed to prevent the zone from becoming too cold. This phenomenon can be seen between 12:00-13:00 hours in Figures 8(b) and 8(c). The MPC controllers in contrast vary the outdoor air ratio and air flow rate as occupancy varies, leading to a lower fan and cooling energy consumption. It should be noted that this reduction in energy use by the MPC controllers requires accurate prediction of occupancy.

From Figure 8(c) it can be seen that *S-MPC* violates the humidity limits during unoccupied hours while *SL-MPC* and *BL* do not. This is because *S-MPC* decides to bring in the slightly cooler outside air in an attempt to provide "free" cooling but fails to realize that the air is humid. If this violation of humidity limit occurs over several months, serious and costly issues such as mold growth are a real possibility [6]. This does not occur with *SL-MPC* as humidity is a part of the problem formulation—the humidity constraint is found to be active be-

tween 18:00-28:00 hours as shown in Figure 8(c).

The difference in energy consumption between *S-MPC* and *SL-MPC* occurs over unoccupied hours. This is another effect of the attempt to use "free" cooling by *S-MPC*. The use of slightly cool, but humid, outdoor air results in the cooling coil always having to reduce the temperature of mixed air and de-humidify it, resulting in high power consumption. In the case of *SL-MPC*, it decides to re-circulate return air and reduce the outdoor air ratio, thereby reducing the amount of de-humidification required. This lowers the cooling coil energy consumption and the overall energy consumption.

5.1.2. Mild day

Figure 9 shows the simulation results for a mild day. It is found that *SL-MPC* consumes the least amount of energy when compared to *S-MPC* and *BL*, as seen in Figure 10. Similar to the results from hot day, there are huge violations in humidity limit during unoccupied hours when using *S-MPC*. The conservative set points in *BL* ensure that the comfort limits are not violated but at the cost of high energy use. Therefore, we discuss only the MPC controllers in further detail here.

As discussed in Section 2, there are four control commands the MPC controllers need to decide. They are m_{sa}, r_{oa}, T_{ca}, and T_{sa}. Since the weather condition is not too cold, there will be no reheat ($T_{sa} = T_{ca}$) and the controllers need to decide the remaining three: m_{sa}, r_{oa}, and T_{ca}. During the occupied hours, it is seen that *S-MPC* decides to keep T_{ca} low enough (at 12.8 $^{\circ}C$) similar to *SL-MPC* due to the high internal heat load, and hence maintains the zone humidity. This behavior is similar to the one seen for a hot-humid day. But, the biggest difference in the decisions made by the two MPC controllers are for r_{oa} and m_{sa}. *S-MPC* decides to use 100% of the slightly cold outside air in an attempt to lower the cooling and fan energy consumption, but fails to realize that it is humid. Whereas *SL-MPC* uses much lesser outside air. As a result, the cooling energy consumed by *S-MPC* is much higher than that consumed by *SL-MPC*, and can be seen between 12:00-17:00 hrs in Figures 9(b) and 9(c).

During unoccupied hours both the MPC controllers decide to bring in 100% outside air, but *SL-MPC* decides to keep T_{ca} lower than the one decided by *S-MPC* to ensure that the air is dehumidified enough before being supplied to the zone.

5.1.3. Cold day

Since the outdoor weather is dry, no matter what decisions are made by a controller, it is unlikely to violate humidity constraints in the building. The energy consumed by the two MPC controllers is almost the same, which is much smaller than that by *BL* (Figure 10). *BL* performs simultaneous heating and cooling in a pronounced manner leading to high energy consumption: the fixed outdoor air ratio combined with the 12.8 $^{\circ}C$ (55 $^{\circ}F$) conditioned air requires usage of cooling energy, additionally reheating is required to keep the building warm enough

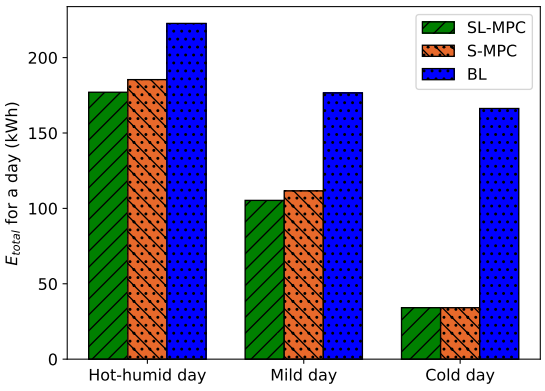

(a) Comparison of total energy consumed over 24 hours by *SL-MPC*, *S-MPC*, and *BL* for different outdoor weather conditions.

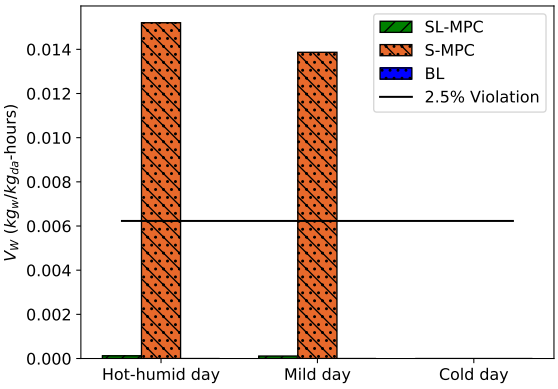

(b) Comparison of humidity violation over 24 hours by *SL-MPC*, *S-MPC*, and *BL* for different outdoor weather conditions. The black line indicates the value of V_W when there is a 2.5% violation over the upper limit of humidity ratio at every instant.

Figure 10: Comparison of controllers' performance.

because of the cold weather. The MPC controllers choose to use as much outdoor air as possible, since the cold outdoor conditions provide free cooling without having to use chilled water.

5.2. Comparison among controllers

The performance metrics discussed in Section 4.3 are computed from simulation data for each of the three controllers, and are shown in Figure 10. The temperature violation V_T was observed to be minimal for all three controllers, and is therefore not shown in the figure. We see from the figure that space humidity is a concern only during hot-humid and mild weather conditions.

Figure 10 shows that *SL-MPC* outperforms the other two controllers: it consumes the least amount of energy under various outdoor weather conditions with negligible violation in thermal comfort constraints.

The simulation results discussed in the previous section show

that *S-MPC* makes decisions that either leads to thermal comfort violations, or higher energy use when compared to *SL-MPC*, under the following conditions.

1. *Mild internal heat load but high outdoor humidity (e.g. spring/summer night)*: In such a condition, *S-MPC* decides that slightly cooler outside air can provide free cooling, but the high humidity of the outside air causes high indoor humidity; see Figures 10(b), 8(c), and 9(c). Thus, *S-MPC* makes decisions in the interest of reducing energy/cost that leads to violation of humidity constraints.
2. *During occupied hours on a mild weather day:* In this case, the *S-MPC* decides to meet the air flow requirement with a larger fraction of outdoor air due to its small sensible heat, failing to recognize its high latent heat. Because of the high internal sensible load during occupied hours, it uses a low conditioned air setpoint which incidentally reduces humidity of the air supplied, so fortunately no space humidity violations occur. However, the decision is energy inefficient compared to the proposed *SL-MPC* controller.

Interestingly, *S-MPC* makes decisions similar to the proposed *SL-MPC* controller either when (i) the internal heat load is high and outdoor weather is hot and humid, or (ii) the outdoor weather is cold and dry. In the latter case, the cold outdoor is used to provide free (sensible) cooling, and since it is dry there is no risk of space humidity becoming large. In the former scenario, *S-MPC* recognizes that the conditioned air temperature must be low enough to maintain the indoor temperature within allowable limits. That decision has an unintended, but good, side effect of maintaining space humidity even though the controller has no knowledge of humidity.

BL uses conservative set points which ensures that there are no violations in humidity and temperature constraints almost all the time, but leads to higher energy use when compared to the two MPC controllers.

These observations provide a basis for a cost-benefit tradeoff analysis of the three controllers. One should first note that the proposed *SL-MPC* requires more sophisticated modeling and additional humidity sensors compared to an MPC controller that ignores humidity/latent heat, and thus is more expensive to use in practice. The additional energy cost savings due to the proposed MPC controller over the naive MPC controller *S-MPC* is small, about 5%; see Figure 10(a). The larger difference is space humidity. As discussed previously, in mild outdoor weather conditions such as spring/summer nights, the proposed MPC controller is able to maintain space humidity constraints while the naive MPC controller leads to poor space humidity. Since this large space humidity occurs over many hours in a night (see Figures 8(c) and 9(c)), and this behavior is likely to repeat every night over the entire season, it may lead to mold growth which can seriously affect occupant health. In fact, additional simulations that are not reported here due to space constraints, show that with larger internal moisture generation, poor space humidity occurs even during occupied hours. Therefore, the benefit of incorporating humidity/latent heat in MPC control of HVAC—or conversely the cost of not doing so—maybe more about occupant health and comfort, and less about energy savings. Additionally, since these benefits (conversely, costs) manifest only over long time periods, experimental evaluations conducted over a short time period, say, less than a few months, may not be adequate to provide a complete assessment.

6. Conclusion

An MPC-based (model predictive control) controller which incorporates humidity and latent heat in a principled manner is presented. Simulations show that the proposed MPC controller outperforms both a naive MPC controller (that does not consider humidity/latent heat) and a baseline rule-based controller in both energy use and thermal comfort, despite large plant-model mismatch. A thorough comparison for several weather conditions indicate the key advantage of the proposed controller over the naive MPC is not energy savings but humidity control. The naive controller may lead to poor humidity control, especially during mild outdoor weather conditions such as spring or summer nights. Such violations in humidity over long periods can cause mold growth and can affect occupant health and comfort.

This study is a first step; there are several avenues for further exploration. A natural extension is to multi-zone buildings. A thorough numerical investigation for various climate zones and HVAC systems is also needed. It may be possible to reformulate the underlying optimization problem in the proposed controller to guarantee feasibility and convexity. Theoretical properties of the controller need to be investigated as well. Another avenue for future work is extension to supply side applications, such as development of humidity-aware HVAC control to provide ancillary services to energy supply networks.

Acknowledgment

This research reported here has been partially supported by the NSF through awards # 1646229 (CPS/ECCS) and # 1934322 (CMMI), and the State of Florida through a REET (Renewable Energy and Energy Efficient Technologies) grant.

References

[1] G. Serale, M. Fiorentini, A. Capozzoli, D. Bernardini, A. Bemporad, Model predictive control (MPC) for enhancing building and HVAC system energy efficiency: Problem formulation, applications and opportunities, Energies 11 (3) (2018) 631 (2018).

[2] P. H. Shaikh, N. B. M. Nor, P. Nallagownden, I. Elamvazuthi, T. Ibrahim, A review on optimized control systems for building energy and comfort management of smart sustainable buildings, Renewable and Sustainable Energy Reviews 34 (2014) 409 – 429 (2014).

[3] S. Qin, T. A. Badgwell, A survey of industrial model predictive control technology, Control Engineering Practice 11 (7) (2003) 733 – 764 (2003).

[4] American Society of Heating, Refrigerating and Air-Conditioning Engineers, ANSI/ASHRAE standard 55-2017, Thermal environmental conditions for human occupancy (2017).

[5] W. S. Duda, Pitfalls of single-fan dual-duct systems in humid climates, ASHRAE Journal 60 (9) (2018) 60–66 (2018).

[6] A. Baughman, E. A. Arens, Indoor humidity and human health–Part I: Literature review of health effects of humidity-influenced indoor pollutants, ASHRAE Transactions 102 Part1 (1996) 192–211 (1996).

[7] J. C. Fischer, C. W. Bayer, Humidity control in school facilities, Energy 30 (35) (2003) 606–613 (2003).

[8] X. Zhou, J. E. Braun, A simplified dynamic model for chilled-water cooling and dehumidifying coils—Part 1: Development (RP-1194), HVAC&R Research 13 (5) (2007) 785–804 (2007).

[9] U.S. DOE, EnergyPlus engineering reference: The reference to EnergyPlus calculations, Lawrence Berkeley National Laboratory (2018) 1–1704 (2018).

[10] S. Klein, W. Beckman, J. Mitchell, J. Duffie, N. Duffie, T. Freeman, et al., Trnsys 17: A transient system simulation program: Mathematical reference, University of Wisconsin: Madison, WI, USA (2009) 1–486 (2009).

[11] S. Goyal, P. Barooah, A method for model-reduction of non-linear thermal dynamics of multi-zone buildings, Energy and Buildings 47 (2012) 332–340 (April 2012).

[12] J. Williams, Why is the supply air temperature 55F?, `http://8760engineeringblog.blogspot.com/2013/02/why-is-supply-air-temperature-55f.html`, last accessed: Aug, 03, 2020 (2013).

[13] D. B. Crawley, L. K. Lawrie, F. C. Winkelmann, W. F. Buhl, Y. J. Huang, C. O. Pedersen, et al., EnergyPlus: creating a new-generation building energy simulation program, Energy and buildings 33 (4) (2001) 319–331 (2001).

[14] ASHRAE, The ASHRAE handbook : Applications (SI Edition) (2011).

[15] N. S. Raman, K. Devaprasad, P. Barooah, MPC-based building climate controller incorporating humidity, in: American Control Conference, 2019, pp. 253–260 (July 2019).

[16] J. B. Rawlings, D. Q. Mayne, M. Diehl, Model Predictive Control: Theory, Computation, and Design, Nob Hill, 2017 (2017).

[17] J. B. Rawlings, D. Angeli, C. N. Bates, Fundamentals of economic model predictive control, in: 51st IEEE Conference on Decision and Control (CDC), 2012, pp. 3851–3861 (Dec 2012).

[18] D. Schwingshackl, J. Rehrl, M. Horn, LoLiMoT based MPC for air handling units in HVAC systems, Building and Environment 96 (2016) 250 – 259 (2016).

[19] J. Mei, X. Xia, M. Song, An autonomous hierarchical control for improving indoor comfort and energy efficiency of a direct expansion air conditioning system, Applied Energy 221 (2018) 450 – 463 (2018).

[20] J. Mei, X. Xia, Energy-efficient predictive control of indoor thermal comfort and air quality in a direct expansion air conditioning system, Applied Energy 195 (2017) 439 – 452 (2017).

[21] X.-C. Xi, A.-N. Poo, S.-K. Chou, Support vector regression model predictive control on a HVAC plant, Control Engineering Practice 15 (8) (2007) 897–908 (2007).

[22] N. Wang, J. Zhang, X. Xia, Desiccant wheel thermal performance modeling for indoor humidity optimal control, Applied Energy 112 (2013) 999–1005 (2013).

[23] S. Goyal, P. Barooah, Energy-efficient control of an air handling unit for a single-zone VAV system, in: IEEE Conference on Decision and Control, 2013, pp. 4796 – 4801 (2013).

[24] S. Goyal, H. Ingley, P. Barooah, Occupancy-based zone climate control for energy efficient buildings: Complexity vs. performance, Applied Energy 106 (2013) 209–221 (June 2013).

[25] S. Goyal, P. Barooah, T. Middelkoop, Experimental study of occupancy-based control of HVAC zones, Applied Energy 140 (2015) 75–84 (February 2015).

[26] M. Kumar, I. N. Kar, Design of model-based optimizing control scheme for an air-conditioning system, HVAC&R Research 16 (5) (2010) 565–597 (2010).

[27] A. E. Ruano, S. Pesteh, S. Silva, H. Duarte, G. Mestre, P. M. Ferreira, et al., The IMBPC HVAC system: A complete MBPC solution for existing HVAC systems, Energy and Buildings 120 (2016) 145–158 (2016).

[28] J. Joe, P. Karava, A model predictive control strategy to optimize the performance of radiant floor heating and cooling systems in office buildings, Applied Energy 245 (2019) 65 – 77 (2019).

[29] X. Chen, Q. Wang, J. Srebric, Occupant feedback based model predictive control for thermal comfort and energy optimization: A chamber experimental evaluation, Applied Energy 164 (2016) 341 – 351 (2016).

[30] Y. Kwak, J.-H. Huh, C. Jang, Development of a model predictive control framework through real-time building energy management system data, Applied Energy 155 (2015) 1 – 13 (2015).

[31] E. Png, S. Srinivasan, K. Bekiroglu, J. Chaoyang, R. Su, K. Poolla, An internet of things upgrade for smart and scalable heating, ventilation and air-conditioning control in commercial buildings, Applied Energy 239 (2019) 408 – 424 (2019).

[32] C. J. Meinrenken, A. Mehmani, Concurrent optimization of thermal and electric storage in commercial buildings to reduce operating cost and demand peaks under time-of-use tariffs, Applied Energy 254 (2019) 113630 (2019).

[33] P. Fanger, Thermal comfort: Analysis and applications in environmental engineering, McGraw-Hill, 1970 (1970).

[34] N. Radhakrishnan, Y. Su, R. Su, K. Poolla, Token based scheduling for energy management in building HVAC systems, Applied Energy 173 (2016) 67 – 79 (2016).

[35] V. M. Zavala, Real-time optimization strategies for building systems, Industrial & Engineering Chemistry Research 52 (9) (2012) 3137–3150 (2012).

[36] Y. Jiang, X. Wang, H. Zhao, L. Wang, X. Yin, L. Jia, Dynamic modeling and economic model predictive control of a liquid desiccant air conditioning, Applied Energy 259 (2020) 114174 (2020).

[37] S. Wang, X. Jin, Model-based optimal control of VAV air-conditioning system using genetic algorithm, Building and Environment 35 (6) (2000) 471–487 (2000).

[38] D. Sturzenegger, D. Gyalistras, M. Morari, R. S. Smith, Model predictive climate control of a Swiss office building: Implementation, results, and cost-benefit analysis, IEEE Transactions on Control Systems Technology 24 (1) (2016) 1–12 (Jan 2016).

[39] J. Široký, F. Oldewurtel, J. Cigler, S. Privara, Experimental analysis of model predictive control for an energy efficient building heating system, Applied Energy 88 (9) (2011) 3079–3087 (September 2011).

[40] S. C. Bengea, A. D. Kelman, F. Borrelli, R. Taylor, S. Narayanan, Implementation of model predictive control for an HVAC system in a mid-size commercial building, HVAC&R Research 20 (2013) 121–135 (2013).

[41] A. Coffman, P. Barooah, Simultaneous identification of dynamic model and occupant-induced disturbance for commercial buildings, Building and Environment 128 (2018) 153–160 (2018).

[42] M. Wetter, P. Haves, A modular building controls virtual test bed for the integration of heterogeneous systems, Proceedings of SimBuild 3 (1) (2008) 69–76 (2008).

[43] N. S. Raman, P. Barooah, On the round-trip efficiency of an HVAC-based virtual battery, ArXiv e-prints ArXiv:1803.02883 (2018) (2018).

[44] American Society of Heating, Refrigerating and Air-Conditioning Engineers, The ASHRAE handbook fundamentals (SI Edition) (2017).

[45] ASHRAE, ANSI/ASHRAE standard 62.1-2016, ventilation for acceptable air quality (2016).

[46] Y. Ma, S. Richter, F. Borrelli, Chapter 14: Distributed model predictive control for building temperature regulation, In Control and Optimiza-

tion with Differential-Algebraic Constraints 22 (2012) 293–314 (March 2012).

[47] J. A. E. Andersson, J. Gillis, G. Horn, J. B. Rawlings, M. Diehl, Casadi: a software framework for nonlinear optimization and optimal control, Mathematical Programming Computation 11 (1) (2019) 1–36 (Mar 2019).

[48] A. Wächter, L. T. Biegler, On the implementation of an interior-point filter line-search algorithm for large-scale nonlinear programming, Mathematical Programming 106 (1) (2006) 25–57 (Mar 2006).

[49] Weather Underground, `https://www.wunderground.com`.

[50] National Solar Radiation Database (NSRDB), `https://nsrdb.nrel.gov`.